

Dynamic Behavior of Intramolecularly Base-Stabilized Phosphatetrylenes. Insights into the Inversion Processes of Trigonal Pyramidal Germanium(II) and Tin(II) Centers

Keith Izod,* John Stewart, Ewan R. Clark, William McFarlane, Ben Allen, William Clegg, and Ross W. Harrington

Main Group Chemistry Laboratories, School of Chemistry, Bedson Building, University of Newcastle, Newcastle upon Tyne, NE1 7RU, U.K.

Received December 11, 2008

The reaction between SnCl_2 and either 1 or 2 equiv of the lithium salt $[\{(\text{Me}_3\text{Si})_2\text{CH}\}(\text{C}_6\text{H}_4\text{-}2\text{-CH}_2\text{NMe}_2)\text{P}\}\text{Li}$ gives the heteroleptic compound $[\{(\text{Me}_3\text{Si})_2\text{CH}\}(\text{C}_6\text{H}_4\text{-}2\text{-CH}_2\text{NMe}_2)\text{P}\}\text{SnCl}$ (**7**) and the homoleptic, intramolecularly base-stabilized diphosphastannylenes $[\{(\text{Me}_3\text{Si})_2\text{CH}\}(\text{C}_6\text{H}_4\text{-}2\text{-CH}_2\text{NMe}_2)\text{P}\}_2\text{Sn}$ (**8**), respectively, in good yields. The solid state structure of **8** shows that the tin(II) center is three-coordinate, bound by the N and P atoms of a chelating phosphide ligand and the P atom of a second phosphide ligand. Both **7** and **8** are highly dynamic in solution. Variable-temperature NMR spectra suggest that compound **7** and its germanium analogue **5** are subject to two distinct dynamic processes in polar solvents, which are attributed to the formation of adducts between either **5** or **7** and the free phosphine $\{(\text{Me}_3\text{Si})_2\text{CH}\}(\text{C}_6\text{H}_4\text{-}2\text{-CH}_2\text{NMe}_2)\text{PH}$ (**9**) and interconversion between diastereomers of these adducts. Adduct formation is observed only in polar solvents and may be associated with the formation of weakly bound $[\{(\text{Me}_3\text{Si})_2\text{CH}\}(\text{C}_6\text{H}_4\text{-}2\text{-CH}_2\text{NMe}_2)\text{P}\}\text{E}(\text{L})]^+ \cdots \text{Cl}^-$ ion pairs in solution. The dynamic behavior of **8** has been studied by multielement and variable-temperature NMR experiments; at high temperatures there is rapid equilibrium between diastereomers, but at low temperatures a single diastereomer predominates and exchange between the chelating and terminal phosphide ligands is frozen out. DFT calculations on the model compound $\{(\text{Me})(\text{C}_6\text{H}_4\text{-}2\text{-CH}_2\text{NMe}_2)\text{P}\}\text{SnCl}$ (**7a**) suggest that epimerization occurs either through a vertex-inversion process at phosphorus [$E_{\text{inv}} = 65.3 \text{ kJ mol}^{-1}$] or an edge-inversion process at tin [$E_{\text{inv}} = 141.0 \text{ kJ mol}^{-1}$], of which the former is clearly favored. DFT calculations on the model complex $\{(\text{Me})(\text{C}_6\text{H}_4\text{-}2\text{-CH}_2\text{NMe}_2)\text{P}\}_2\text{Sn}$ (**8a**) indicate that the lowest energy dynamic process involves exchange between the chelating and terminal phosphide ligands via a pseudotrigonal bipyramidal intermediate [$E = -12.6 \text{ kJ mol}^{-1}$]. Inversion at tin in **8a** (via an unusual hybrid edge/vertex-inversion process) is calculated to have a barrier of $206.3 \text{ kJ mol}^{-1}$, whereas the barriers to vertex-inversion at phosphorus are 59.4 and 51.0 kJ mol^{-1} for the chelating and terminal phosphorus atoms, respectively.

Introduction

Stable diaminetetrylenes, $(\text{R}_2\text{N})_2\text{E}$ [$\text{E} = \text{Si}, \text{Ge}, \text{Sn}, \text{Pb}$], were first reported by Lappert and co-workers in the 1970s, and since then, examples of these compounds have become relatively numerous.^{1–4} In contrast, examples of the corresponding diphosphatetrylenes, $(\text{R}_2\text{P})_2\text{E}$, remain somewhat scarce. Crystallographically characterized diphosphatetrylenes are limited to just a very few examples: the dimeric compounds $\{(\text{iBu})_2\text{P}\}_2\text{Pb}$,⁵ $\{(\text{Me}_3\text{Si})_2\text{P}\}_2\text{Pb}$,⁶ and $\{(\text{iPr}_2\text{P})_2\text{Ge}\}_2$ ⁷ and the monomeric compounds $[\{(\text{Tripp})_2\text{FSi}\}(\text{iPr}_3\text{Si})\text{P}\}_2\text{E}$ [$\text{E} = \text{Ge}, \text{Sn}$ (**1**), Pb ; $\text{Tripp} = 2,4,6\text{-iPr}_3\text{C}_6\text{H}_2$];⁸ Driess and co-workers have also recently reported the crystal structures of the heteroleptic β -diketiminato-supported

phosphagermylenes $[\text{CH}\{(\text{CMe})(2,6\text{-iPr}_2\text{C}_6\text{H}_3\text{N})\}_2]\text{Ge}(\text{PR}_2)$ [$\text{PR}_2 = \text{PH}_2, \text{PH}(\text{SiMe}_3), \text{P}(\text{SiMe}_3)_2, 1/2(\text{PH-PH})$].⁹ In addition, Power and co-workers recently reported the synthesis and spectroscopic characterization of the monomeric diphosphastannylenes $[\{2,6\text{-}$

* Corresponding author. E-mail: k.j.izod@ncl.ac.uk.

(1) For reviews see: (a) Barrau, J.; Rima, G. *Coord. Chem. Rev.* **1998**, *178–180*, 593. (b) Tokitoh, N.; Okazaki, R. *Coord. Chem. Rev.* **2000**, *210*, 251. (c) Kira, M. *J. Organomet. Chem.* **2004**, *689*, 4475. (d) Weidenbruch, M. *Eur. J. Inorg. Chem.* **1999**, 373. (e) Klinkhammer, K. W. In *Chemistry of Organic Germanium, Tin and Lead Compounds*; Rappoport, Z., Ed.; Wiley: New York, 2002; Vol. 2, pp 283–357. (f) Veith, M. *Angew. Chem., Int. Ed. Engl.* **1987**, *26*, 1.

(2) For reviews of N-heterocyclic silylenes see: (a) Hill, N. J.; West, R. *J. Organomet. Chem.* **2004**, *689*, 4165. (b) Gehrhuis, B.; Lappert, M. F. *J. Organomet. Chem.* **2001**, *617*, 209.

(3) For a review of N-heterocyclic germylenes see: Kühn, O. *Coord. Chem. Rev.* **2004**, *248*, 411.

(4) For leading references to diamidogermylenes, -stannylenes, and -plumbylenes see: (a) Fjeldberg, T.; Hope, H.; Lappert, M. F.; Power, P. P.; Thorne, A. J. *J. Chem. Soc., Chem. Commun.* **1983**, 639. (b) Olmstead, M. M.; Power, P. P. *Inorg. Chem.* **1984**, *23*, 413. (c) Tang, Y.; Felix, A. M.; Zakharov, L. N.; Rheingold, A. L.; Kemp, R. A. *Inorg. Chem.* **2004**, *43*, 7239. (d) Avent, A. G.; Drost, C.; Gehrus, B.; Hitchcock, P. B.; Lappert, M. F. *Z. Anorg. Allg. Chem.* **2004**, *630*, 2090. (e) Gans-Eichler, T.; Gudat, D.; Nieger, M. *Angew. Chem., Int. Ed.* **2002**, *41*, 1888. (f) Chorley, R. W.; Hitchcock, P. B.; Lappert, M. F.; Leung, W.-P.; Power, P. P.; Olmstead, M. M. *Inorg. Chim. Acta* **1992**, *198*, 203. (g) Braunschweig, H.; Hitchcock, P. B.; Lappert, M. F.; Pierssens, L. J.-M. *Angew. Chem., Int. Ed. Engl.* **1994**, *33*, 1156. (h) Lappert, M. F.; Slade, M. J.; Atwood, J. L.; Zaworotko, M. J. *J. Chem. Soc., Chem. Commun.* **1980**, 621. (i) Bazinet, P.; Yap, G. P. A.; Richeson, D. S. *J. Am. Chem. Soc.* **2001**, *123*, 11162.

(5) Cowley, A. H.; Giolando, D. M.; Jones, R. A.; Nunn, C. M.; Power, J. M. *Polyhedron* **1988**, *7*, 1909.

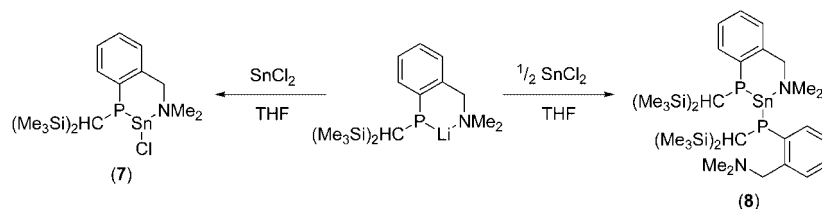
(6) Goel, S. C.; Chiang, M. Y.; Rauscher, D. J.; Buhro, W. E. *J. Am. Chem. Soc.* **1993**, *115*, 160.

(7) Druckenbrodt, C.; du Mont, W.-W.; Ruthe, F.; Jones, P. G. *Z. Anorg. Allg. Chem.* **1998**, *624*, 590.

(8) Driess, M.; Janoschek, R.; Pritzkow, H.; Rell, S.; Winkler, U. *Angew. Chem., Int. Ed.* **1995**, *34*, 1614.

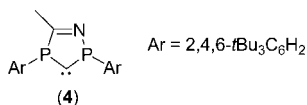
(9) Yao, S.; Brym, M.; Merz, K.; Driess, M. *Organometallics* **2008**, *27*, 3601.

Scheme 1



(2,4,6- $\text{Me}_3\text{C}_6\text{H}_2$) $_2\text{C}_6\text{H}_3$ }(Ph)P $_2$ Sn (2).¹⁰ The ate complexes $(t\text{Bu}_2\text{P})\text{E}(\mu-t\text{Bu}_2\text{P})_2\text{Li}(\text{THF})$ [E = Sn (3), Pb]¹¹ and several homometallic Sn(II) phosphinidene clusters and heterometallic Ca/Sn or Ba/Sn phosphide and phosphinidene clusters have also been reported.¹²

The scarcity of diphosphatetrylenes may, at least in part, be attributed to the perception that $p\pi-p\pi$ interactions between the vacant tetrel p-orbital and the lone pairs at phosphorus would be poor and, thus, that the electron deficiency of the tetrel center would be alleviated to only a very limited extent in these compounds. This situation contrasts with the excellent $p\pi-p\pi$ overlap found in diaminotetrylenes, which contributes significantly to the stability of these species. However, it has been calculated that the inherent π -donor capability of phosphorus is at least as great as that of nitrogen.¹³ The poor P-E $p\pi-p\pi$ overlap in diphosphatetrylenes is largely a consequence of the considerable barrier to inversion of phosphorus and the attendant difficulty in achieving the planar configuration necessary for optimal $p\pi-p\pi$ interactions. However, such planarity may be promoted by a range of strategies, including the use of sterically demanding substituents at the pnictogen center and/or incorporation of the heteroatoms into a cyclic system; these strategies were recently employed by Bertrand and co-workers in their landmark synthesis of the first P-heterocyclic carbene, **4**.¹⁴ With particular relevance to the current report, it has also been demonstrated previously that electropositive substituents, e.g., SiR_3 , significantly lower the barrier to inversion of tertiary phosphine and arsine centers.¹⁵



We recently reported the synthesis and dynamic behavior of the intramolecularly base-stabilized phosphagermylenes $[(\text{Me}_3\text{Si})_2\text{CH}](\text{C}_6\text{H}_4-2-\text{CH}_2\text{NMe}_2)\text{PGeCl}$ (5) and $[(\text{Me}_3\text{Si})_2\text{CH}]-$

$(\text{C}_6\text{H}_4-2-\text{CH}_2\text{NMe}_2)\text{P}]_2\text{Ge}$ (6).¹⁶ Multielement and variable-temperature NMR experiments clearly showed that inversion at phosphorus is a relatively low energy process in these compounds and that, consequently, interconversion between diastereomers is rapid on the NMR time scale at room temperature. We now report the synthesis and characterization of the tin(II) analogues of **5** and **6** and present NMR and theoretical data concerning the dynamic behavior of these species.

Results and Discussion

Synthesis and Structural Characterization. The reaction between SnCl_2 and 1 equiv of the lithium phosphide $[(\text{Me}_3\text{Si})_2\text{CH}](\text{C}_6\text{H}_4-2-\text{CH}_2\text{NMe}_2)\text{P}[\text{Li}]$ in THF gives the heteroleptic phosphastannylene $[(\text{Me}_3\text{Si})_2\text{CH}](\text{C}_6\text{H}_4-2-\text{CH}_2\text{NMe}_2)\text{P}[\text{SnCl}]$ (7) in good yield as a pale yellow, light-, heat-, and air-sensitive, microcrystalline solid after workup (Scheme 1). Although initially crystallized from cold diethyl ether, once isolated, compound **7** is essentially insoluble in most common organic solvents, including THF, but is sufficiently soluble in dichloromethane to permit spectroscopic characterization (see below). Due to its very low solubility, in spite of repeated attempts, we were unable to obtain single crystals of **7** suitable for X-ray crystallography; however, the identity of **7** was unambiguously confirmed by elemental analysis and multielement (^1H , $^{13}\text{C}\{^1\text{H}\}$, $^{31}\text{P}\{^1\text{H}\}$, and $^{119}\text{Sn}\{^1\text{H}\}$) NMR spectroscopy. Attempts to derivatize **7** in order to obtain a soluble compound more amenable to characterization have so far failed: treatment of **7** with a variety of alkylating agents such as NpLi , NpMgBr , and Np_2Zn (Np = neopentyl) led to deposition of elemental tin and formation of either the free phosphine $[(\text{Me}_3\text{Si})_2\text{CH}](\text{C}_6\text{H}_4-2-\text{CH}_2\text{NMe}_2)\text{PH}$ or the known diphosphine $[(\text{Me}_3\text{Si})_2\text{CH}](\text{C}_6\text{H}_4-2-\text{CH}_2\text{NMe}_2)\text{P}]_2$.

The reaction between SnCl_2 and 2 equiv of *in situ* generated $[(\text{Me}_3\text{Si})_2\text{CH}](\text{C}_6\text{H}_4-2-\text{CH}_2\text{NMe}_2)\text{P}[\text{Li}]$ in THF gives the diphosphastannylene $[(\text{Me}_3\text{Si})_2\text{CH}](\text{C}_6\text{H}_4-2-\text{CH}_2\text{NMe}_2)\text{P}]_2\text{Sn}$ (8) in good yield (Scheme 1). The ready synthesis of **8** contrasts markedly with the corresponding reaction between GeI_2 and 2 equiv of $[(\text{Me}_3\text{Si})_2\text{CH}](\text{C}_6\text{H}_4-2-\text{CH}_2\text{NMe}_2)\text{P}[\text{Li}]$, which, under the same conditions, gives the ate complex $[(\text{Me}_3\text{Si})_2\text{CH}](\text{C}_6\text{H}_4-2-\text{CH}_2\text{NMe}_2)\text{P}]_2\text{Ge} \cdot \text{Li}_2\text{I}_2(\text{OEt}_2)_2$; the homoleptic diphosphagermylene **6** may be prepared by the reaction between GeI_2 and 2 equiv of the potassium salt $[(\text{Me}_3\text{Si})_2\text{CH}](\text{C}_6\text{H}_4-2-\text{CH}_2\text{NMe}_2)\text{P}[\text{K}]$.¹⁶ In contrast to **7**, compound **8** is soluble in both ethereal and hydrocarbon solvents; deep orange single crystals of **8** were obtained from cold *n*-hexane. Like **7** compound **8** has limited thermal and photolytic stability; whereas the corresponding diphosphagermylene **6** is stable at elevated temperatures, compound **8** begins to decompose above 50 °C in solution or on exposure to ambient light.

Compound **8** is chiral at both phosphorus centers and at the germanium atom; it crystallizes as discrete monomers in the

(10) Rivard, E.; Sutton, A. D.; Fettinger, J. C.; Power, P. P. *Inorg. Chim. Acta* **2007**, *360*, 1278.

(11) Arif, A. M.; Cowley, A. H.; Jones, R. A.; Power, J. M. *J. Chem. Soc., Chem. Commun.* **1986**, 1446.

(12) For examples see: (a) Westerhausen, M.; Hausen, H.-D.; Schwarz, W. Z. *Anorg. Allg. Chem.* **1996**, *622*, 903. (b) Westerhausen, M.; Krofta, M.; Wiberg, N.; Nöth, H.; Pflitzner, A. Z. *Naturforsch. B* **1998**, *53*, 1489. (c) Westerhausen, M.; Hausen, H.-D.; Schwarz, W. Z. *Anorg. Allg. Chem.* **1995**, *621*, 877. (d) Westerhausen, M.; Krofta, M.; Schneiderbauer, S.; Piotrowski, H. Z. *Anorg. Allg. Chem.* **2005**, *631*, 1391. (e) Allan, R. E.; Beswick, M. A.; Cromhout, N. L.; Paver, M. A.; Raithby, P. R.; Trevithick, M.; Wright, D. S. *Chem. Commun.* **1996**, 1501. (f) Garcia, F.; Hahn, J. P.; McPartlin, M.; Pask, C. M.; Rothenberger, A.; Stead, M. L.; Wright, D. S. *Organometallics* **2006**, *25*, 3275.

(13) Kapp, J.; Schade, C.; El-Nahasa, A. M.; Schleyer, P. von R.; *Angew. Chem., Int. Ed. Engl.* **1996**, *35*, 2236.

(14) Martin, D.; Baceiredo, A.; Gornitzka, H.; Schoeller, W. W.; Bertrand, G. *Angew. Chem., Int. Ed.* **2005**, *44*, 1700.

(15) (a) Beachler, R. D.; Casey, J. P.; Cook, R. J.; Senkler, G. H., Jr.; Mislow, K. J. *Am. Chem. Soc.* **1987**, *109*, 338. (b) Beachler, R. D.; Mislow, K. J. *Am. Chem. Soc.* **1971**, *93*, 773. (c) Beachler, R. D.; Andose, J. D.; Stackhouse, J.; Mislow, K. J. *Am. Chem. Soc.* **1972**, *94*, 8060. (d) Driess, M.; Merz, K.; Monse, C. Z. *Anorg. Allg. Chem.* **2000**, *626*, 2264.

(16) Izod, K.; McFarlane, W.; Allen, B.; Clegg, W.; Harrington, R. W. *Organometallics* **2005**, *24*, 2157.

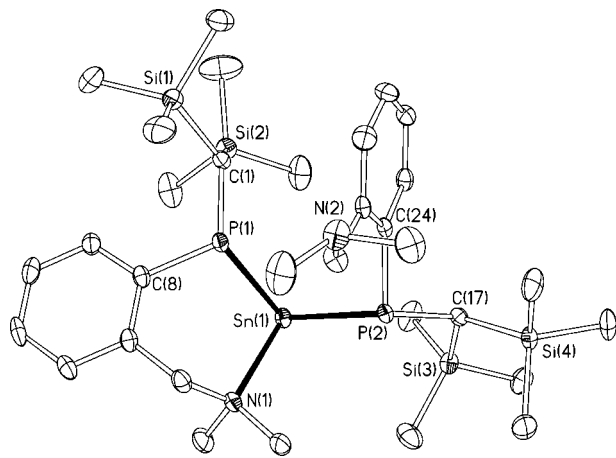


Figure 1. Molecular structure of one of the two independent molecules of **8** with 40% probability ellipsoids and with H atoms omitted for clarity. Selected bond lengths (Å) and angles (deg) [values for the second molecule in square brackets]: Sn(1)–P(1) 2.5906(9) [Sn(2)–P(3) 2.6061(9)], Sn(1)–P(2) 2.6407(8) [Sn(2)–P(4) 2.6439(9)], Sn(1)–N(1) 2.422(3) [Sn(2)–N(3) 2.379(3)], P(1)–C(1) 1.865(3) [P(3)–C(33) 1.872(3)], P(1)–C(8) 1.821(3) [P(3)–C(40) 1.833(3)], P(2)–C(17) 1.892(3) [P(4)–C(49) 1.895(3)], P(2)–C(24) 1.846(3) [P(4)–C(56) 1.848(3)], P(1)–Sn(1)–N(1) 83.66(7) [P(3)–Sn(2)–N(3) 85.92(8)], P(1)–Sn(1)–P(2) 90.80(3) [P(3)–Sn(2)–P(4) 94.55(3)], N(1)–Sn(1)–P(2) 92.76(7) [N(3)–Sn(2)–P(4) 93.44(8)], C(1)–P(1)–C(8) 108.69(15) [C(33)–P(3)–C(40) 107.33(15)], C(1)–P(1)–Sn(1) 112.74(11) [C(33)–P(3)–Sn(2) 107.91(11)], C(8)–P(1)–Sn(1) 97.02(11) [C(40)–P(3)–Sn(2) 98.02(11)], C(17)–P(2)–C(24) 102.18(14) [C(49)–P(4)–C(56) 101.95(15)], C(17)–P(2)–Sn(1) 112.64(10) [C(49)–P(4)–Sn(2) 110.33(10)], C(24)–P(2)–Sn(1) 101.47(10) [C(56)–P(4)–Sn(2) 100.95(10)].

space group $P\bar{1}$ with two crystallographically independent molecules of identical $\text{Sn}_R\text{P}^{ch}_R\text{P}'_R$ stereochemistry in the asymmetric unit (where P^{ch} and P' refer to the phosphorus atoms of the chelating and terminal phosphide ligands, respectively), which differ only trivially in their bond lengths and angles. The molecular structure of **8** is shown in Figure 1, along with selected bond lengths and angles. One phosphide ligand binds the tin(II) center through its P and N atoms, forming a puckered, six-membered chelate ring, while the second phosphide ligand binds the tin center solely through its phosphorus atom; the lone pair of the amino group of this second ligand is directed away from the tin atom. The tin center is thus three-coordinate and adopts a trigonal-pyramidal geometry due to the presence of a stereochemically active lone pair [sum of angles at Sn = 267.22° (273.91° in the second molecule)].

The Sn–P distances to the chelating and terminal phosphide ligands, 2.5906(9) and 2.6407(8) Å, respectively [2.6061(9) and 2.6439(9) Å, respectively, in the second molecule in the asymmetric unit], are similar to the Sn–P distances in **1** [2.567(1) Å]⁸ and **3** [2.684(4), 2.702(3), and 2.671(4) Å].¹¹ The P–Sn–N bite angle of the chelating ligand [83.66(7)°; 85.92(8)° in the second molecule] is significantly smaller than the corresponding angle in the germanium analogue **6** [97.49(3)°],¹⁶ consistent with the larger size of tin compared to germanium. The phosphorus atoms in both the chelating and terminal ligands are distinctly pyramidal [sum of angles at P(1) 315.45°, P(2) 316.29°, P(3) 313.26°, P(4) 313.23°], suggesting very little P–Sn $p\pi$ – $p\pi$ overlap, consistent with intramolecular base stabilization of the Sn(II) center.

During the course of this work we had cause to prepare again the heteroleptic phosphagermylene **5** (see below).¹⁶ Although we had previously been unable to obtain crystals of this

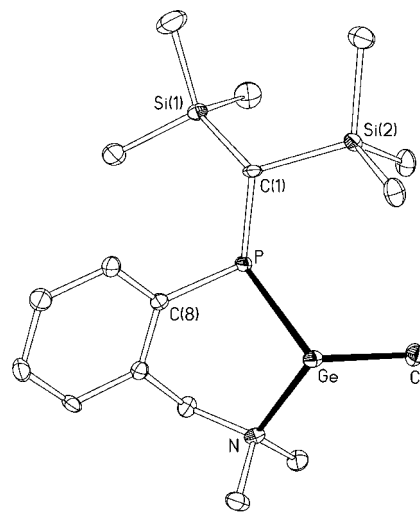


Figure 2. Molecular structure of **5** with 40% probability ellipsoids and with H atoms omitted for clarity. Selected bond lengths (Å) and angles (deg): Ge–P 2.4205(16), Ge–N 2.191(5), Ge–Cl 2.2965(16), P–C(1) 1.866(6), P–C(8) 1.842(6), P–Ge–Cl 99.42(6), P–Ge–N 88.70(13), N–Ge–Cl 95.73(14), Ge–P–C(1) 112.74(19), Ge–P–C(8) 87.14(17), C(1)–P–C(8) 103.6(3).

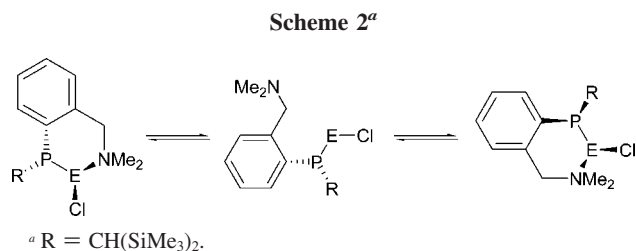
compound suitable for X-ray crystallography, we now find that single crystals may be obtained by slow evaporation of a saturated solution of **5** in diethyl ether at room temperature. The structure of **5** is shown in Figure 2, along with selected bond lengths and angles.

Compound **5** is chiral at both the germanium and phosphorus centers and crystallizes as a monomeric species possessing a Ge_RP_S configuration. The germanium atom is coordinated by the P and N centers of a chelating phosphide ligand [P–Ge–N bite angle 88.70(13)°] and by a chloride ligand, affording the germanium center a highly pyramidal geometry [sum of angles at Ge = 283.85°]. The Ge–P distance of 2.4205(16) Å is slightly longer than the Ge–P distances in the homoleptic compound **6** [Ge–P 2.4023(4) and 2.4114(4) Å],¹⁶ but is similar to Ge–P distances in related compounds containing divalent germanium; for example, the Ge–P distances in $\{(i\text{Pr}_2\text{P})_2\text{Ge}\}_2$ range from 2.3981(11) to 2.4261(11) Å,⁷ whereas the Ge–P distance in $[\text{CH}\{(\text{CMe})(2,6\text{-}i\text{Pr}_2\text{C}_6\text{H}_3\text{N})\}_2]\text{Ge}\{\text{PH}(\text{SiMe}_3)\}_2$ is 2.4261(7) Å.⁹ The Ge–Cl distance of 2.2965(16) Å is similar to other Ge(II)–Cl distances; for example, the Ge–Cl distance in $\text{GeCl}_2(1,4\text{-dioxane})$ is 2.2813(5) Å,¹⁷ whereas the Ge–Cl distance in $[\text{HC}\{\text{CMeN}(2,6\text{-}i\text{Pr}_2\text{C}_6\text{H}_3)\}_2]\text{GeCl}$ is 2.295(12) Å.¹⁸ Although the Ge–Cl vectors of adjacent molecules in the unit cell are aligned in an antiparallel fashion to give an elongated Ge_2Cl_2 parallelogram, the intermolecular Ge...Cl distances are 4.535(2) Å, and so it is unlikely that there are any significant intermolecular Ge...Cl interactions. For comparison, the Ge...Cl distance between the essentially unassociated GeCl_2 units in $\text{GeCl}_2(1,4\text{-dioxane})$ is 3.463(1) Å.¹⁷

Solution Behavior of the Heteroleptic Phosphatetrylenes 5 and 7. Compounds **5** and **7** exhibit highly unusual dynamic behavior in solution, which we attribute to a combination of (i) inversion processes that interconvert the diastereomers of these compounds and (ii) the formation of adducts between the tetrylenes and the free phosphine $\{(\text{Me}_3\text{Si})_2\text{CH}\}(\text{C}_6\text{H}_4\text{-2-}$

(17) Denk, M. K.; Khan, M.; Lough, A. J.; Shuchi, K. *Acta Crystallogr. Sect. C* **1998**, C54, 1830.

(18) Ding, Y.; Roesky, H. W.; Noltemeyer, M.; Schmidt, H.-G.; Power, P. P. *Organometallics* **2001**, 20, 1190.



CH₂NMe₂)PH (**9**). The evidence to support this proposal is presented below.

We have previously shown that the epimerization of intramolecularly base-stabilized heteroleptic phosphatetrylenes such as **5** may potentially proceed through (i) inversion at the tetrel center via a planar transition state, (ii) inversion at the tetrel center via E–N dissociation, rotation about the E–P bond, and subsequent E–N recoordination (Scheme 2; E = Ge, Sn, Pb), and/or (iii) inversion at the phosphorus center. Theoretical calculations suggest that, for compound **5**, the favored epimerization pathway is inversion at phosphorus, rather than at germanium. We were interested to see what effect the increased atomic number of the tetrel center in **7** would have on such processes and so have undertaken a variable-temperature NMR study of this compound. To our knowledge, the inversion of trigonal-pyramidal tin(II) species has not previously been probed; the diastereomeric nature of **7** and **8** and the relative ease with which dynamic processes may be studied by ³¹P NMR spectroscopy make these potentially excellent compounds for gaining insight into such processes.

Once isolated in the solid state, compound **7** is almost completely insoluble in most common organic solvents, including THF; however, **7** dissolves sufficiently, although still rather sparingly, in CD₂Cl₂ to obtain reasonable NMR spectra. Compound **7** is readily hydrolyzed and decomposes on extended exposure to ambient light or elevated temperatures, yielding the free phosphine **9** as the only spectroscopically identifiable product (we assume that the tin-containing byproduct of hydrolysis is an insoluble tin hydroxide or oxide species that cannot be observed spectroscopically, whereas thermolysis/photolysis of **7** yields elemental tin). The combination of the extremely limited solubility of **7** and its ready decomposition has the consequence that NMR signals due to sparingly soluble **7** are always accompanied by signals due to the free phosphine **9**, which is produced in small quantities as a byproduct of decomposition during sample preparation, but which has a much greater solubility than **7**; in spite of our extensive experience in the handling of highly air-sensitive materials, we were unable to prepare a sample of **7** completely free from contamination by **9**. However, this contamination revealed rather unexpected dynamic behavior for **7** and its germanium analogue **5**, which is described below.

The room-temperature ³¹P{¹H} NMR spectrum of **7** in CD₂Cl₂ consists of two very broad, overlapping singlets centered at –41.1 (A) and –34.3 ppm (B), on which ¹¹⁷Sn/¹¹⁹Sn satellites are not resolved, along with a sharp singlet at –69.5 ppm (C) due to **9** (Figure 3). As the temperature is reduced, peaks A and B sharpen and move to higher field, until, at –30 °C, the spectrum consists of a sharp singlet at –43.3 ppm (A) exhibiting satellites due to coupling to ^{117/119}Sn (*J*_{PSn} = 1056 Hz) along with a lower intensity, broader singlet at –36.0 ppm (B) (*J*_{PSn} = 1249 Hz). As the temperature is reduced further, signal A sharpens and moves upfield slightly, while signal B broadens and continues to shift to significantly higher field, until, at –69 °C, peaks A and B lie at –44.6 and –40.1 ppm, respectively,

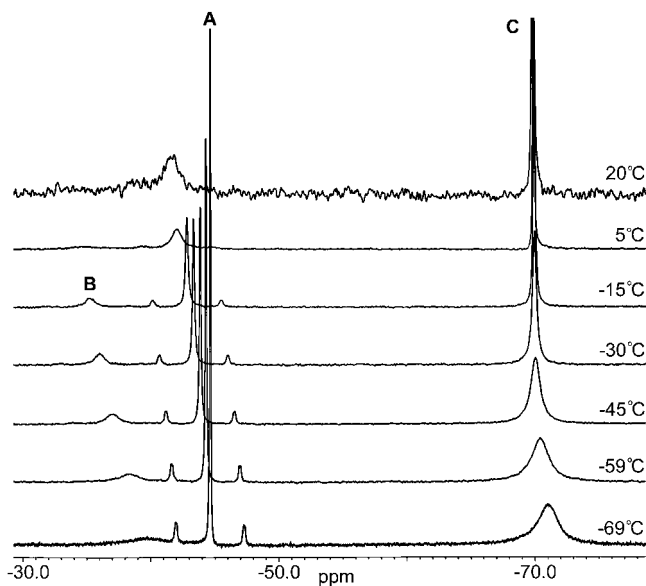


Figure 3. Variable-temperature ³¹P{¹H} NMR spectra of **7** in CD₂Cl₂.

in an approximately 3:1 ratio. At the same time peak C broadens and shifts to higher field, such that, at –69 °C, this peak lies at –71.0 ppm ($\Delta\nu_{1/2}$ = 340.3 Hz) [cf. –70.9 ppm ($\Delta\nu_{1/2}$ = 7.7 Hz) for pure **9** at room temperature in this solvent]. A low-temperature ³¹P EXSY spectrum indicates that, at –41 °C, whereas the two species responsible for signals A and B are undergoing rapid dynamic exchange, neither of these species is exchanging with the free phosphine **9**. In this context it is notable that the variable-temperature ³¹P{¹H} NMR spectra of pure **9** in CD₂Cl₂ are invariant over the temperature range 20 to –80 °C, confirming that the broadening of peak C in the ³¹P{¹H} spectra of **7** is a direct consequence of the presence of the stannylene.

The room-temperature ¹H NMR spectrum of **7** in CD₂Cl₂ consists of a single set of rather broad ligand resonances, consistent with the presence of a single ligand environment on the NMR time scale, along with a set of sharp signals due to **9**. At this temperature the diastereotopic N-methyl groups in **7** give rise to a pair of equal intensity, very broad singlets, indicating that the nitrogen center is not undergoing inversion and must, therefore, be coordinated to the tin atom. As the temperature is reduced, the signals due to **7** broaden and decoalesce, until, at –80 °C, the spectrum exhibits two distinct sets of ligand resonances in the approximate ratio 1.7:1. This is most clearly manifested in the SiMe₃ region of the spectrum, which contains, in addition to signals due to **9**, four singlets at –0.02, 0.09, 0.15, and 0.25 ppm, in the ratio 1:1.7:1.7:1, due to the diastereotopic CH(SiMe₃)₂ groups.

The room-temperature ¹¹⁹Sn{¹H} spectrum of **7** in CD₂Cl₂ consists of a broad doublet at 257 ppm (*J*_{PSn} = 1070 Hz). At –41 °C the spectrum consists of a sharp doublet at 249 ppm (*J*_{PSn} = 1102 Hz); no other signals are observed at this temperature.

Although compound **7** is only very sparingly soluble in THF once isolated, it proved possible to obtain variable-temperature ³¹P{¹H} NMR data on the crude reaction mixture when **7** was prepared in this solvent. Variable-temperature ³¹P{¹H} NMR spectra of the crude THF solution (containing a small amount of *d*₈-toluene) exhibit similar characteristics to those obtained from solutions in CD₂Cl₂. At –66 °C the spectrum exhibits two

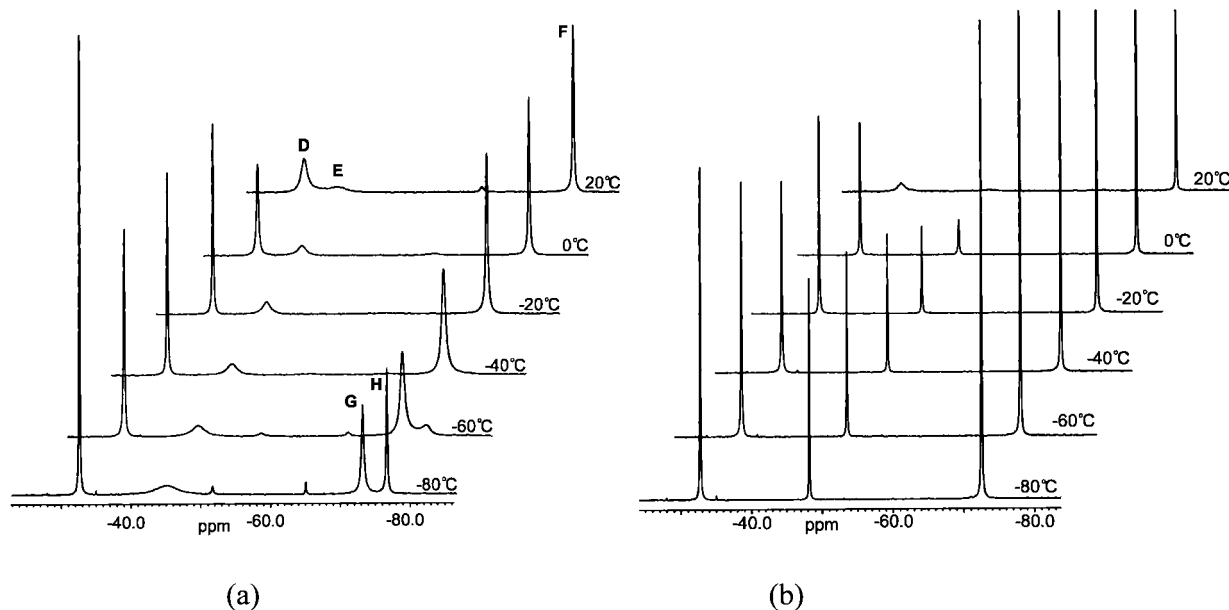


Figure 4. Variable-temperature $^{31}\text{P}\{^1\text{H}\}$ NMR spectra of (a) a mixture of **5** and **9** in CD_2Cl_2 and (b) a mixture of **5** and **9** in the presence of an excess of NEt_3 in CD_2Cl_2 .

signals due to **7** at -48.0 and -49.2 ppm, while the free phosphine signal lies at -72.1 ppm ($\Delta\nu_{1/2} = 12.5$ Hz).

The variable-temperature ^1H and $^{31}\text{P}\{^1\text{H}\}$ NMR spectra of **7** in both CD_2Cl_2 and THF are clearly consistent with the presence of two distinct phosphastannylene species, which are undergoing rapid dynamic exchange at room temperature. At low temperatures this exchange process is frozen out and signals for both species are evident, although one species (A) clearly predominates.

However, the low-temperature line broadening associated with the free phosphine **9** was rather unexpected and suggests that a second dynamic process is operating. No such line broadening was observed in the variable-temperature $^{31}\text{P}\{^1\text{H}\}$ spectra of the germanium analogue **5** in d_8 -toluene (in which the stannylene **7** is insoluble). This prompted us to investigate the behavior of **5** in the presence of the free phosphine **9** in CD_2Cl_2 ; the increased solubility of **5** also enabled us to study this system in somewhat greater detail than the relatively insoluble stannylene **7** (see below).

The room-temperature $^{31}\text{P}\{^1\text{H}\}$ NMR spectrum of a mixture of **5** and **9** in CD_2Cl_2 exhibits broad signals at -31.8 (D) and -36.9 ppm (E), due to the phosphagermylene, along with a sharp singlet at -70.5 ppm (F), due to **9** (Figure 4a). As the temperature is reduced, peak D sharpens and remains at essentially the same chemical shift, while peak E broadens and moves upfield. Simultaneously, peak F broadens, moves upfield, and decoalesces into two broad singlets G and H. Thus, at -80 °C, the $^{31}\text{P}\{^1\text{H}\}$ spectrum consists of a sharp singlet at -32.6 (D), a broad singlet at -44.6 (E), a moderately broad singlet at -73.2 (G), and a sharp singlet at -76.7 ppm (H); in the absence of proton decoupling, these latter signals are resolved as doublets [$J_{\text{PH}} = 222.4$ Hz (G), 206.0 Hz (H)], clearly identifying these signals as arising from secondary phosphine species. A ^{31}P EXSY spectrum of a mixture of **5** and **9** in CD_2Cl_2 at -70 °C indicates that exchange between species D and E and between species G and H is rapid, but that there is no exchange between the pairs D/E and G/H at this temperature.

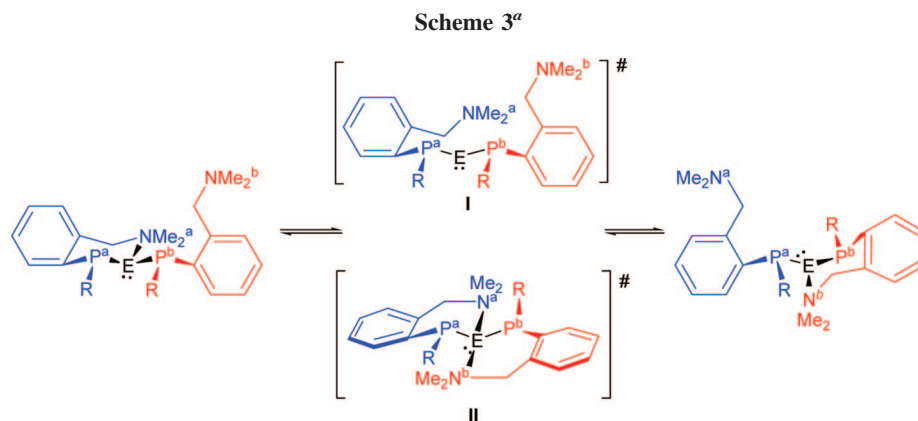
Thus, in d_8 -toluene compound **5** appears to be subject to a dynamic equilibrium between two species (most likely diastereomers), which does not appear to involve the free phosphine **9**.¹⁶ In polar solvents (CD_2Cl_2 or THF) both **5** and **7** are subject

to a dynamic equilibrium between two species; although this equilibrium does involve the free phosphine, it does not involve direct exchange between either **5** or **7** and **9**. The NMR data suggest that the dynamic behavior observed for **5** and **7** in CD_2Cl_2 may be attributed to two distinct processes: formation of an adduct between **5** or **7** and the free phosphine **9** and dynamic exchange between the diastereomers of these adducts.

The upfield shift in the position of the phosphine resonances in these spectra suggests that both of the possible stereoisomers of **5** (or **7**) form an adduct with **9**. Since the free phosphine is itself chiral, each adduct possesses three stereocenters, and thus the adducts may exist in up to four diastereomeric forms. In the $^{31}\text{P}\{^1\text{H}\}$ spectra of a mixture of **5** and **9** (Figure 4a), the broad signals E and G observed at low temperature may be assigned to the phosphide and phosphine ligands, respectively, of one adduct diastereomer and the sharp peaks D and H may be assigned to the phosphide and phosphine ligands of a second stereoisomer. Whereas peaks D and H remain sharp at low temperature, peaks E and G broaden and move to higher field. This is consistent with further decoalescence of signals E and G and suggests that adduct E:G is undergoing moderately fast epimerization, which we were unable to freeze out due to the low temperature that this would require. In contrast, adduct D:H does not exhibit this behavior; either D:H is present as a single diastereomer or else epimerization of this diastereomer is rapid on the NMR time scale at -80 °C and so only an averaged signal is observed.

Unfortunately, with the available data it is not possible to identify unambiguously the nature of these adducts. However, the lack of any resolved ^{31}P – ^{31}P coupling (cf. the $^{31}\text{P}\{^1\text{H}\}$ spectra of **6** and **8** (see below)) suggests that the adduct is formed via a $\text{Ge}\cdots\text{N}$, rather than a $\text{Ge}\cdots\text{P}$, interaction between the tetrylene and the free phosphine; it is likely that a $\text{Ge}\cdots\text{P}$ interaction would also be disfavored on steric grounds.

It is notable that there is no evidence for the formation of adduct species in the NMR spectra of **5** in d_8 -toluene (nor in the spectra of the homoleptic diphosphatetrylenes **6** and **8** in this solvent (see below)).⁸ The peaks due to residual **9** in these spectra lie at the same position as that of a pure sample



^a R = CH(SiMe₃)₂.

of **9** (i.e., in the absence of tetrylene species) and remain invariant over a wide temperature range, suggesting that adduct formation occurs only in the presence of a polar solvent. In this regard, it has been suggested by Barrau and co-workers that the closely related, three-coordinate, heteroleptic, β -diketiminato-supported halogermynes {PhNC(Me)CHC(Me)NPh}GeX [X = Cl, I] may be regarded as weakly bonded {PhNC(Me)CHC(Me)NPh}Ge⁺...X⁻ ions.¹⁹ Consistent with this, it has been shown by Power and co-workers that treatment of the sterically hindered β -diketiminato-supported halogermylene {ArNC(Me)CHC(Me)NAr}GeX with B(C₆F₅)₃ in the presence of water readily yields the ion pair [{ArNC(Me)CHC(Me)NAr}Ge][(HO)B(C₆F₅)₃] [Ar = 2,6-*i*Pr₂C₆H₃].^{20a} With this in mind, we tentatively suggest that adduct formation in the present case may be associated with the formation of weakly bonded [{{(Me₃Si)₂CH}(C₆H₄-2-CH₂NMe₂)P}E(L)]⁺...Cl⁻ ion pairs in solution [E = Ge, Sn; L = **9**]. Adduct formation may then be attributed to the enhanced Lewis acidity of the pseudo-two-coordinate tetrylene center in the putative cationic tetrylene intermediate [{{(Me₃Si)₂CH}(C₆H₄-2-CH₂NMe₂)P}E]⁺. It is likely that [{{(Me₃Si)₂CH}(C₆H₄-2-CH₂NMe₂)P}E(L)]⁺...Cl⁻ ion pairs would be significantly stabilized in polar solvents, whereas the formation of such species would be inhibited in nonpolar solvents, consistent with our observation that broadening of the signal due to **9** occurs only in the presence of **5** or **7** in CD₂Cl₂ or THF.

In order to obtain further evidence to support this proposal, we undertook an NMR-scale experiment in which the free phosphine **9** was allowed to compete for the germanium center in **5** with the strong base NEt₃. The room-temperature ³¹P{¹H} NMR spectrum of a mixture of **5** and **9** in CD₂Cl₂, in the presence of an excess of NEt₃, contains two broad singlets at -31.5 and -44.5 ppm due to phosphagermylene species, along with a sharp singlet at -70.9 ppm due to **9** (Figure 4b). As the temperature is reduced, these three signals merely sharpen, without any significant changes in chemical shift. This strongly suggests that, under these conditions, NEt₃ competes successfully for the Lewis acidic germanium center and thus that the signals observed at -31.5 and -44.5 ppm may be attributed to the two diastereomers of the adduct [{{(Me₃Si)₂CH}(C₆H₄-2-CH₂NMe₂)P}Ge(Cl)(NMe₃)] [or of the weakly bonded adduct ion pair [{{(Me₃Si)₂CH}(C₆H₄-2-CH₂NMe₂)P}Ge(NMe₃)⁺...Cl⁻], neither of which interacts with **9**. Thus, the

presence of NEt₃ appears to inhibit the formation of an adduct between **5** and **9**.

Solution Behavior of the Diphosphastannylene 8. In addition to the inversion processes (i–iii) accessible to **7**, compound **8** may undergo two further exchange processes: (iv) inversion at the terminal, rather than the chelating, phosphorus center and (v) exchange between the chelating and terminal phosphide ligands. This latter process may proceed either via a two-coordinate transition state (i.e., via a dissociative mechanism, I) or via a four-coordinate, pseudotrigonal-bipyramidal transition state (i.e., via an associative mechanism, II) (Scheme 3). Exchange via either mechanism may have two potential outcomes, depending on the sense of the chelate ring formed during this process, resulting in either retention or inversion of stereochemistry at the tin center. For the dissociative mechanism, both outcomes are equally possible; however, for the associative mechanism the two possible pseudotrigonal-bipyramidal transition states differ considerably. The approach of N^b on an axis bisecting the two phosphorus atoms generates a transition state in which the two phosphorus centers occupy equatorial sites and would, upon cleavage of the N^a–Sn bond, lead to exchange of P^a and P^b with retention of configuration at tin. In contrast, the approach of N^b on an axis bisecting N^a and P^b results in a transition state in which the phosphorus centers occupy an axial and an equatorial site and would lead to inversion at tin on cleavage of the N^a–Sn bond. Clearly, this latter pathway is likely to be significantly disfavored on steric grounds, and so we propose that exchange of the amino groups in **8** via an associative pathway would most likely occur with retention of configuration at tin (i.e., without interconversion of the diastereomers).

The ³¹P{¹H} spectrum of **8** in *d*₈-toluene at 50 °C consists of a very broad singlet at -49.3 ppm, exhibiting poorly resolved satellites due to coupling to ^{117/119}Sn (*J*_{PSn} ≈ 1090 Hz) [we were unable to obtain a good-quality spectrum of **8** at this temperature due to its limited thermal stability]. As the temperature is reduced, this signal broadens and begins to decoalesce, until, at -40 °C, the spectrum consists of two sharp doublets at -49.1 and -59.5 ppm, each exhibiting poorly resolved satellites due to coupling to tin (*J*_{PP} = 47.4 Hz; *J*_{PSn} = 1124 and 898 Hz, respectively), consistent with the presence of distinct chelating and terminal ligand environments at this temperature (Figure 5). Below -40 °C the ³¹P{¹H} spectra of **8** do not change significantly.

The room-temperature ¹H NMR spectrum of **8** in *d*₈-toluene exhibits a single set of ligand resonances, consistent with rapid exchange between the chelating and terminal phosphide

(19) Saur, I.; Miqueu, K.; Rima, G.; Barrau, J.; Lemierre, V.; Chrostowska, A.; Sotiropoulos, J.-M.; Pfister-Guillouzo, G. *Organometallics* **2003**, *22*, 3143.

(20) (a) Stender, M.; Phillips, A. D.; Power, P. P. *Inorg. Chem.* **2001**, *40*, 5314. (b) Driess, M.; Yao, S.; Brym, M.; van Wullen, C. *Angew. Chem., Int. Ed.* **2006**, *45*, 4349.

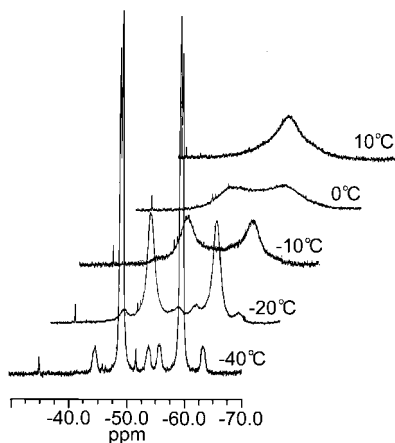


Figure 5. Variable-temperature $^{31}\text{P}\{^1\text{H}\}$ NMR spectra of **8** in d_8 -toluene.

ligands on the NMR time scale. The spectrum consists of broad singlets at 0.00 and 0.17 ppm due to the diastereotopic SiMe_3 groups, a doublet ($J_{\text{PH}} = 6.4$ Hz) at 0.68 ppm due to the methine protons, a singlet at 2.13 ppm due to the NMe_2 groups, two very broad singlets at ~ 3.50 and 3.94 ppm due to the CH_2N protons, and a series of multiplets in the range 6.72–7.52 ppm due to the aryl protons. As the temperature is reduced, these signals broaden and decoalesce until, at -60 °C, the spectrum exhibits two separate sets of signals in a 1:1 ratio, due to the chelating and terminal phosphide ligands. The diastereotopic SiMe_3 groups give rise to four equal intensity signals at -0.16 , 0.00, 0.06, and 0.19 ppm, while the $\text{CH}(\text{SiMe}_3)_2$ protons give rise to singlets at -1.71 and 0.93 ppm. The diastereotopic NMe_2 groups of the chelating phosphide ligand give rise to two equal intensity signals at 1.35 and 2.24 ppm, and the NMe_2 group of the terminal ligand exhibits a single singlet of twice the intensity at 2.15 ppm due to rapid inversion of the free amino group. The benzylic protons of the terminal ligand give rise to a typical AB pattern ($J_{\text{HH}} = 14.35$ Hz) centered at 4.24 and 4.09 ppm, the latter signal exhibiting further coupling to phosphorus ($J_{\text{PH}} = 4.25$ Hz), whereas the CH_2N protons of the chelating ligand give rise to complex multiplets at 1.99 and 3.58 ppm; the signals due to the aromatic protons lie in the range 6.25–7.82 ppm. The simplicity of the low-temperature ^1H and $^{31}\text{P}\{^1\text{H}\}$ spectra of **8** clearly implies that a single diastereomer predominates at low temperatures.

The large chemical shift difference of 2.64 ppm between the $\text{CH}(\text{SiMe}_3)_2$ protons observed at low temperature and the unusually high-field shift (-1.71 ppm) of one of these protons may be attributed to the orientation of these groups with respect to the aromatic rings of the ligands. In the diastereomer observed by X-ray crystallography the methine proton [H(1)] of the chelating phosphide ligand lies directly over the plane of the aromatic ring of the terminal ligand at a distance of 2.68 Å, and so this proton should experience a strong upfield shift due to ring current effects. In contrast, the methine proton [H(17)] of the terminal ligand lies close to the plane of the same aromatic ring and so should experience an opposite ring current effect to H(1), i.e., a moderate downfield shift. This strongly suggests that the diastereomer observed in the low-temperature ^1H NMR spectrum of **8** has the same configuration as that observed crystallographically.

The variable-temperature ^1H and $^{31}\text{P}\{^1\text{H}\}$ NMR spectra of **8** may potentially be explained as arising from a single diastere-

omer of **8**, which is present in solution at all temperatures and which has an essentially identical structure to that observed in the solid state; the only dynamic process operating in this case would be interconversion between the chelating and terminal phosphide ligands. An alternative explanation for the behavior of **8** is that, in addition to the chelating–terminal ligand exchange, a second dynamic process is operating at high temperatures that involves epimerization via inversion at one or both of the phosphorus centers and/or at the tin atom. DFT studies (see below) suggest that **8** lies on a fairly shallow potential energy surface and that the barriers to epimerization of this compound are low, and so rapid exchange between diastereomers is likely. At low temperatures only the most stable of these diastereomers is observed.

We note that the heteroleptic compound **7** is highly dynamic in solution and that the low-temperature $^{31}\text{P}\{^1\text{H}\}$ spectra of **6**, the germanium analogue of **8**, clearly show the presence of multiple diastereomers.¹⁶ In addition, previous NMR studies have shown that stannyl substituents favor more rapid inversion at phosphorus than germyl substituents (see below). The foregoing, in combination with the DFT studies presented below, suggests that the presence of a single diastereomer of **8** in solution at room temperature is somewhat unlikely. Thus, we propose that the variable-temperature ^1H and $^{31}\text{P}\{^1\text{H}\}$ NMR spectra of **8** are consistent with rapid interconversion on the NMR time scale both between diastereomers and between the chelating and terminal phosphide ligands at room temperature and suggest that epimerization is a lower energy, faster process than exchange between the chelating and terminal ligands. This allows rapid equilibration of the diastereomers, but the relative stability of one of these has the consequence that, at low temperatures, a single diastereomer predominates in which exchange between the chelating and terminal ligands is frozen out.

The significant differences between the dynamic behavior of **8** and **6** may be attributed to the different electronegativities of Sn(II) and Ge(II). It has been shown previously that electro-positive substituents such as SiMe_3 or GeMe_3 significantly reduce the barrier to inversion at trigonal-pyramidal phosphorus centers.¹⁵ For example, it has been reported that line-shape analysis of the variable-temperature ^1H NMR spectra of $i\text{-PrPhP}(\text{GeMe}_3)$ and $i\text{-PrPhP}(\text{CMe}_3)$ yield $\Delta G^\ddagger = 89.5$ and 136.8 kJ mol^{-1} , respectively, for the phosphorus-inversion process.^{15b} The barrier to inversion at phosphorus decreases further with decreasing electronegativity of the substituents, such that, for $i\text{-PrPhP}(\text{SnMe}_3)$ $\Delta G^\ddagger = 80.8$ kJ mol^{-1} . Thus, inversion at phosphorus in **8** should be more energetically favorable than in **6**.

Line-shape analysis of the variable-temperature $^{31}\text{P}\{^1\text{H}\}$ NMR spectra of **8** yields values of $\Delta H^\ddagger = 37 \pm 1$ kJ mol^{-1} and $\Delta S^\ddagger = -50 \pm 3$ $\text{J K}^{-1} \text{mol}^{-1}$ for the chelating–terminal phosphide exchange process in this molecule. The substantial negative entropy of activation is consistent with the formation of the pseudotrigonal-bipyramidal transition state required for chelating–terminal ligand exchange via an associative mechanism (see Scheme 3), whereas the moderate enthalpy of activation may be attributed to the significant reorganization energy associated with the formation of this transition state and the substantial steric congestion present therein.

DFT Calculations. We have carried out a series of DFT calculations in order to gain insight into the barriers to inversion at the phosphorus and tin centers in both **7** and **8**. In all cases final geometries were obtained using the B3LYP hybrid

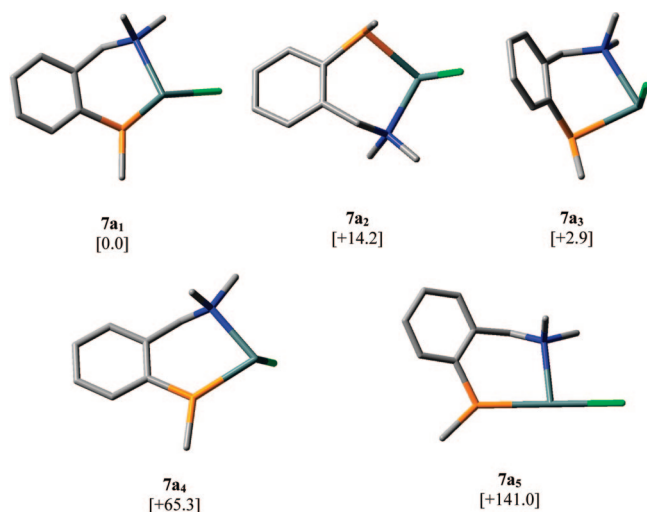
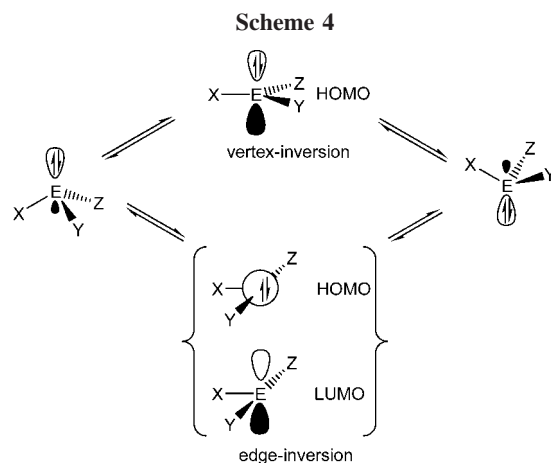


Figure 6. Optimized geometries of the three calculated minima of **7a** (**7a₁**–**7a₃**) and of the transition states for vertex-inversion at phosphorus (**7a₄**) and edge-inversion at tin (**7a₅**), with relative energies (kJ mol⁻¹) in square brackets; H atoms omitted for clarity.

functional,²¹ with a Lan12dz effective core potential basis set on tin²² and an all-electron 6-31G(d,p) basis set on the remaining atoms.²³ The location of minima and transition states was confirmed by the absence or presence of one, imaginary vibrational frequency, respectively; for transition states the principal displacement vectors of the imaginary vibrational mode were consistent with the appropriate inversion processes in each case.

In order to determine the barriers to epimerization of **7** and **8**, we have used the model compounds {Me(C₆H₄-2-CH₂NMe₂)P}-SnCl (**7a**) and {Me(C₆H₄-2-CH₂NMe₂)P}₂Sn (**8a**), to save on computational resources. Replacement of the sterically demanding (Me₃Si)₂CH groups with small Me substituents is likely to significantly underestimate the impact of steric effects on the inversion processes studied. However, the model compounds retain the overall structural skeletons of **7** and **8**, and so we believe that it is possible to draw meaningful conclusions regarding the dynamic processes of these compounds from their models. In order that we might compare the results of the present study directly with those of our previous investigations into the corresponding germanium compounds, we have also calculated single-point energies at the B3LYP/6-31G(d,p) level of theory for the previously obtained geometries of the ground and transition states of the model compounds {Me(C₆H₄-2-CH₂NMe₂)P}GeCl (**5a**) and {Me(C₆H₄-2-CH₂NMe₂)P}₂Ge (**6a**).

For **7a** we have located three minima of very similar energies, which represent the ground state (Sn₅P₅, **7a₁**), its phosphorus-inverted epimer (Sn₅P_R, **7a₂**), and an enantiomer of **7a₂** in which the chlorine atom lies in close proximity to the aromatic ring of the phosphide ligand (Sn_RP₅, **7a₃**) (Figure 6); minima **7a₂** and **7a₃** lie just 14.2 and 2.9 kJ mol⁻¹ higher in energy than the ground state, respectively. As a consequence of the foregoing, we also located a third minimum energy configuration for the



germanium compound (**5a₁**) that has a Ge_RP_R configuration; the two other minima, Ge₅P_R (**5a₂**) and Ge_RP₅ (**5a₃**), diastereomers of **5a₁**, were located in our previous study [relative energies (B3LYP/6-31G(d,p)): **5a₁** 11.7, **5a₂** 16.3, **5a₃** 0.0 kJ mol⁻¹].¹⁶

Previous theoretical studies have indicated that the substitution patterns of tertiary pnictines profoundly affect the mechanism of inversion at the pnictine center. Two inversion mechanisms have been identified: classical inversion via a trigonal-planar transition state (vertex-inversion) and inversion via a T-shaped transition state (edge-inversion) (Scheme 4).²⁴ It is widely regarded that for tertiary pnictines the HOMO in trigonal-planar transition states consists largely of a lone pair located in a pure p-orbital on the pnictogen atom of a₂' symmetry, which lies perpendicular to the plane of the molecule, whereas the HOMO in T-shaped transition states consists of an essentially s-type lone pair of a₁' symmetry located on the pnictogen atom; the LUMO in T-shaped transition states consists of a vacant pnictogen p-orbital that lies perpendicular to the plane of the molecule. Previous studies have shown that in pnictine systems electronegative, σ -withdrawing ligands, such as F, favor edge-inversion, whereas electropositive ligands, such as H, favor vertex-inversion. In addition, ligands that themselves possess lone pairs may potentially stabilize T-shaped transition states through π -donation into the vacant pnictogen p-orbital.

Calculations by Arduengo and Dixon indicate that, whereas vertex-inversion of PH₃ has a barrier of 146.0 kJ mol⁻¹, edge-inversion has a barrier of 670.0 kJ mol⁻¹; in contrast, the barriers to vertex- and edge-inversion processes for PF₃ are calculated to be 356.9 and 225.1 kJ mol⁻¹, respectively.^{24c} In our previous report we suggested that a similar preference exists for the valence isoelectronic germanium(II) center in the trigonal-pyramidal phosphagermylenes **5** and **6**: whereas **6** favors a vertex-inversion process, **5**, which contains an electronegative chloride ligand, favors an edge-inversion process.¹⁶

For the heteroleptic phosphastannylene **7a** transition states corresponding to epimerization of the ground state diastereomer were located for both vertex-inversion at phosphorus (**7a₄**) and edge-inversion at the tin center (**7a₅**) (see Figure 6). We were unable to locate transition states corresponding to vertex-inversion at tin or edge-inversion at phosphorus, optimizations

(21) (a) Becke, A. D. *J. Chem. Phys.* **1993**, *98*, 5648. (b) Stephens, P. J.; Devlin, F. J.; Chablowksi, C. F.; Frisch, M. J. *J. Phys. Chem.* **1994**, *98*, 11623. (c) Hertwig, R. H.; Koch, W. *Chem. Phys. Lett.* **1997**, *268*, 345. (22) (a) Hay, P. J.; Wadt, W. R. *J. Chem. Phys.* **1985**, *82*, 270. (b) Wadt, W. R.; Hay, P. J. *J. Chem. Phys.* **1985**, *82*, 284. (c) Hay, P. J.; Wadt, W. R. *J. Chem. Phys.* **1985**, *82*, 299.

(23) (a) Hariharan, P. C.; Pople, J. A. *Theor. Chim. Acta* **1973**, *28*, 213. (b) Francl, M. M.; Pietro, W. J.; Hehre, W. J.; Binkley, J. S.; Gordon, M. S.; DeFrees, D. J.; Pople, J. A. *J. Chem. Phys.* **1982**, *77*, 3654.

(24) (a) Dixon, D. A.; Arduengo, A. J., III; Fukunaga, T. *J. Am. Chem. Soc.* **1986**, *108*, 2461. (b) Dixon, D. A.; Arduengo, A. J., III *J. Chem. Soc., Chem. Commun.* **1987**, 498. (c) Dixon, D. A.; Arduengo, A. J., III *J. Am. Chem. Soc.* **1987**, *109*, 338. (d) Schwerdtfeger, P.; Laakkonen, L. J.; Pyykkö, P. *J. Chem. Phys.* **1992**, *96*, 6807. (e) Schwerdtfeger, P.; Hunt, P. *Adv. Mol. Struct. Res.* **1999**, *5*, 223. (f) Schwerdtfeger, P.; Boyd, P. D. W.; Fischer, T.; Hunt, P.; Liddell, M. *J. Am. Chem. Soc.* **1994**, *116*, 9620. (g) Göller, A.; Clark, T. *Chem. Commun.* **1997**, 1033.

always converging to **7a₅** and **7a₄**, respectively. Similarly, we were unable to locate a transition state containing a two-coordinate tin center, corresponding to inversion at the Sn center via Sn–N dissociation/Sn–P rotation/Sn–N recoordination (see Scheme 2), optimizations consistently converging to transition state **7a₅**; this is consistent with our NMR observations, which indicate that dissociation of the NMe₂ group is slow on the NMR time scale. It is notable that in our previous study of **5a** we were similarly unable to locate the corresponding transition states for these latter processes. The calculated inversion processes for the tin and phosphorus centers in **7a** are consistent with both Arduengo and Dixon's and our own previous observations regarding the effect of electronegative substituents on the favorability of edge- and vertex-inversion processes.

Transition state **7a₄**, corresponding to inversion at phosphorus via a vertex-inversion process, is 65.3 kJ mol⁻¹ higher in energy than the ground state **7a₁**. This compares with a barrier to inversion at phosphorus of 84.9 kJ mol⁻¹ for the germanium analogue **5a** at the same level of theory. The lower barrier to phosphorus inversion in the phosphastannylene **7a** compared to the phosphagermylene **5a** is again consistent with previous observations that electropositive substituents lower the barrier to vertex-inversion of tertiary pnictines (see above).

Transition state **7a₅**, corresponding to inversion of the tin center via an edge-inversion process, is 141.0 kJ mol⁻¹ higher in energy than the ground state **7a₁**, and this process is clearly disfavored in comparison to inversion at phosphorus via transition state **7a₄**. For comparison, the corresponding barrier to inversion at germanium in **5a** is 179.1 kJ mol⁻¹. The lower barrier to inversion at tin compared to germanium is consistent with previous calculations, which suggest that, whereas the barrier to vertex-inversion of tertiary pnictines increases with increasing atomic number, edge-inversion follows the opposite trend. For example, the barriers to vertex-inversion of PH₃, AsH₃, and SbH₃ are calculated to be 146.0, 172.8, and 179.1 kJ mol⁻¹, respectively, whereas the barriers to edge-inversion of PF₃, AsF₃, and SbF₃ have been calculated as 225.1, 193.7, and 161.9 kJ mol⁻¹, respectively.^{24c} By analogy, the edge-inversion barrier for the tin center in phosphastannylene **7a**, which is valence isoelectronic with a tertiary stibine, should be lower than the edge-inversion barrier for the germanium center in the phosphagermylene **5a**, which is valence isoelectronic with a tertiary arsine.

The tin atom in **7a₅** deviates only marginally from a strictly T-shaped geometry. The P, Sn, N, and Cl atoms are coplanar and the P–Sn–Cl angle is 180.0°; however, the P–Sn–N angle is less than 90° due to constraints associated with chelate ring formation (P–Sn–N 83.05°). The phosphorus center in **7a₅** approaches planarity (sum of angles at phosphorus = 349.84°), although this atom is somewhat more pyramidal than that in the corresponding transition state for **5a** (sum of angles at phosphorus = 359.98°). The planarity of the phosphorus atoms in **5a** and **7a** is entirely consistent with an edge-inversion mechanism, in which the transition state is stabilized by $p\pi$ – $p\pi$ interactions between the lone pairs at phosphorus and the vacant p -orbital on the tetrel center (see Scheme 4). The more pyramidal nature of the phosphorus atom in **7a₅** compared to **5a₅** may be attributed to less efficient overlap between the lone pair on phosphorus and the large, diffuse 5 p -orbital on Sn in the former compared with overlap between the phosphorus lone pair and the vacant 4 p -orbital on Ge in the latter.

Minima were located for all four diastereomers of the model compound **8a**; these minima differ in energy by less than 16 kJ mol⁻¹ (Figure 7). The ground state diastereomer **8a₁** adopts a

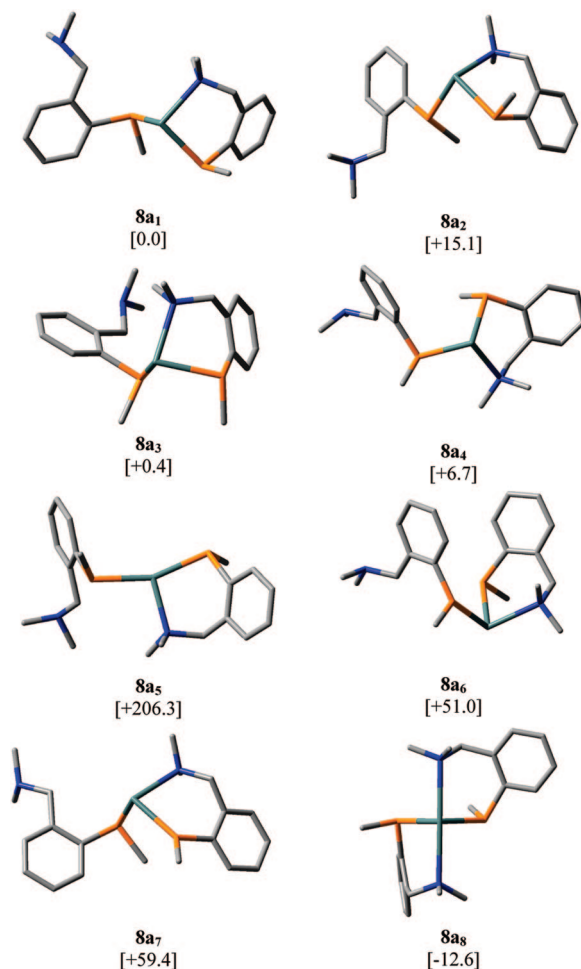


Figure 7. Optimized geometries of the four calculated minima of **8a** (**8a₁**–**8a₄**), the calculated transition states for inversion at tin (**8a₅**), P' (**8a₆**), and P^{ch} (**8a₇**), and the pseudotrigonal-bipyramidal intermediate (**8a₈**), with relative energies (kJ mol⁻¹) in square brackets; H atoms omitted for clarity.

$\text{Sn}_3\text{P}^{\text{ch}}_R\text{P}'_S$ configuration, although the $\text{Sn}_3\text{P}^{\text{ch}}_R\text{P}'_R$ stereoisomer (**8a₂**), corresponding to the structure of **8** observed crystallographically, lies just 15.1 kJ mol⁻¹ higher in energy [the difference in chirality designations between **8** and **8a** arises from the replacement of the (Me₃Si)₂CH group in the former with a Me group in the latter]. The $\text{Sn}_3\text{P}^{\text{ch}}_S\text{P}'_S$ (**8a₃**) and $\text{Sn}_R\text{P}^{\text{ch}}_R\text{P}'_S$ (**8a₄**) diastereomers lie 0.4 and 6.7 kJ mol⁻¹ above the ground state, respectively.

Unexpectedly, all attempts to obtain a transition state for inversion at tin converged to transition state **8a₅**, in which the tin atom adopts a planar geometry midway between trigonal planar and T-shaped (P–Sn–P angle 157.73°, Figure 7). We were unable to locate a transition state corresponding to either pure edge- or pure vertex-inversion at the tin center for this compound. For comparison, a trigonal-planar transition state was located for inversion at the germanium center in **6a**. The barrier to inversion at tin via this hybrid edge/vertex-inversion mechanism is 206.3 kJ mol⁻¹; this compares with a barrier to inversion at germanium in **6a** via a vertex-inversion mechanism of 191.2 kJ mol⁻¹. The similarity of these two inversion barriers appears to be a consequence of the differing inversion mechanisms in each case, since, by analogy with the valence isoelectronic tertiary pnictines, the barrier to inversion via a vertex-inversion process should increase, whereas the barrier

to inversion via an edge-inversion process should decrease with increasing atomic number of the tetrel center.

As we found for **7a**, we were unable to locate transition states corresponding to edge-inversion of either the chelating or terminal phosphorus centers in **8a**, consistent with the presence of the electropositive tin atom. The barriers to vertex-inversion of the phosphorus centers in the terminal (**8a₆**) and chelating (**8a₇**) ligands are calculated to be 51.0 and 59.4 kJ mol⁻¹, respectively; these values are substantially lower than those calculated for the corresponding transition states in the germanium analogue **6a** (88.3 and 101.7 kJ mol⁻¹, respectively). This is consistent with our variable-temperature NMR results, which indicate that interconversion between diastereomers is more facile for **8** than for **6**, and with previous NMR studies on the inversion of tetrel-substituted tertiary pnictines (see above).

Attempts to locate a transition state containing a two-coordinate tin center, corresponding to the transition state for exchange between the chelating and terminal phosphide ligands via a dissociative pathway, were unsuccessful; these calculations consistently converged to give a four-coordinate pseudotrigonal-bipyramidal tin center (**8a₈**), corresponding to the transition state for phosphide ligand exchange via an associative pathway. A similar situation was found for the germanium analogue **6a**, and in keeping with our previous findings, at the B3LYP level of theory, **8a₈** is a minimum, rather than a transition state, with a calculated energy 12.6 kJ mol⁻¹ more stable than the “ground state” **8a₁**. This implies that chelating–terminal ligand exchange is favored over inversion at tin or phosphorus and runs counter to our NMR observations, which suggest that, for **8**, chelating–terminal ligand exchange is less energetically favorable than epimerization. Clearly, the steric bulk associated with the (Me₃Si)₂CH substituents should significantly disfavor the formation of a pseudotrigonal-bipyramidal intermediate, and thus exchange of the chelating and terminal ligands should be disfavored with respect to the alternative epimerization processes. Indeed, it is likely that an increase in steric bulk at the tin and phosphorus centers in both **7** and **8** will result in increased planarization of these atoms and a consequent reduction in the barrier to inversion at these centers.

Conclusions

Multielement and variable-temperature NMR spectroscopy reveals that the intramolecularly base-stabilized phosphatrylenes **5** and **7** are highly dynamic in solution. DFT calculations indicate that, for these compounds, epimerization at the phosphorus centers via a vertex-inversion process is significantly favored over epimerization via an edge-inversion process at the tetrel centers. NMR spectroscopy also reveals that **5** and **7** are somewhat Lewis acidic, forming adducts with the free phosphine **9** in polar solvents such as CD₂Cl₂ and THF. These adducts appear to be formed through E⋯NMe₂ contacts (E = Ge, Sn) between the tetrel center and the amino group of the free phosphine; in the presence of triethylamine the formation of adducts between the phosphatrylene and **9** is inhibited. Adduct formation is not observed in nonpolar solvents, and so we tentatively propose that the adducts consist of weakly associated [[{(Me₃Si)₂CH}(C₆H₄-2-CH₂NMe₂)P]E(**9**)]⁺⋯Cl⁻ ion pairs, which are stabilized in polar solvents.

The diphosphastannylene **8** is also highly dynamic in solution. Multielement and variable-temperature NMR studies, combined with DFT calculations, suggest that the lowest energy dynamic process is epimerization at the terminal phosphorus center via a vertex-inversion process, although exchange between the chelating and terminal phosphide ligands is also a relatively

low-energy process. Indeed, DFT calculations on the model complex **8a** suggest that the intermediate in the chelating–terminal ligand exchange process, which contains a pseudotrigonal-bipyramidal tin center, is 12.6 kJ mol⁻¹ more stable than the “ground state” diastereomer containing one chelating and one terminal phosphide ligand.

Experimental Section

All manipulations were carried out using standard Schlenk techniques under an atmosphere of dry nitrogen. Diethyl ether, THF, *n*-hexane, and light petroleum (bp 40–60 °C) were dried prior to use by distillation under nitrogen from sodium, potassium, or sodium/potassium alloy. THF was stored over activated 4 Å molecular sieves; diethyl ether, *n*-hexane, and light petroleum were stored over a potassium film. Deuterated toluene was distilled from potassium, and CD₂Cl₂ was distilled from CaH₂; NMR solvents were deoxygenated by three freeze–pump–thaw cycles and were stored over activated 4 Å molecular sieves. Tin(II) chloride was dried with chlorotrimethylsilane prior to use. The compounds [(Me₃Si)₂CH](C₆H₄-2-CH₂NMe₂)P]Li²⁵ and [(Me₃Si)₂CH](C₆H₄-2-CH₂NMe₂)P]GeCl (**5**)¹⁶ were prepared by a previously published procedure; single crystals of **5** were isolated by slow evaporation of a freshly prepared, saturated solution of this compound in diethyl ether at room temperature. All other compounds were used as supplied by the manufacturer.

¹H and ¹³C{¹H} NMR spectra were recorded on a JEOL Lambda500 spectrometer operating at 500.16 and 125.65 MHz, respectively, or a Bruker Avance300 spectrometer operating at 300.15 and 75.47 MHz, respectively; chemical shifts are quoted in ppm relative to tetramethylsilane. ³¹P{¹H} NMR spectra were recorded on a JEOL Lambda500 or a JEOL Eclipse270 spectrometer operating at 202.47 and 109.37 MHz, respectively, and ¹¹⁹Sn{¹H} NMR spectra were recorded on a JEOL Lambda500 spectrometer operating at 186.50 MHz; ³¹P and ¹¹⁹Sn chemical shifts are quoted in ppm relative to external 85% H₃PO₄ and external Me₄Sn, respectively. Phase-sensitive ³¹P EXSY spectra were obtained at a measuring frequency of 202.47 MHz without proton decoupling using a standard 90°–*t*₁–90°–*τ*_m–90°Acq(*t*₂) pulse sequence with 1024 data points in the *t*₂ dimension and 128 in *t*₁ and with a mixing time of 40 ms. Elemental analyses were obtained by the Elemental Analysis Service of London Metropolitan University.

[[{(Me₃Si)₂CH}(C₆H₄-2-CH₂NMe₂)P]SnCl (**7**). To a stirred solution of SnCl₂ (0.59 g, 3.11 mmol) in cold (–78 °C) THF (20 mL) was added a solution of [(Me₃Si)₂CH](C₆H₄-2-CH₂NMe₂)P]Li (1.03 g, 3.11 mmol) in THF (20 mL), excluding light as much as possible. The reaction mixture was allowed to attain room temperature and was stirred for 16 h. Solvent was removed *in vacuo*, and the residue was extracted into Et₂O (20 mL) and filtered. The filtrate was cooled to –30 °C for 16 h, giving yellow crystals of **7**. Yield: 1.07 g, 72%. Anal. Calcd for C₁₆H₃₁NPSi₂SnCl: C, 40.14; H, 6.53; N, 2.93. Found: C, 40.07; H, 6.62; N, 2.86. ¹H NMR (CD₂Cl₂, 20 °C): δ 0.19 (s, 18H, SiMe₃), 1.02 (s, 1H, CHP), 2.25 (s, 3H, NMe₂), 2.77 (s, 3H, NMe₂), (s, 2H, CH₂N) 7.07–7.29 (m, 4H, aryl). ¹³C{¹H} NMR (CD₂Cl₂, 22 °C): δ 2.63 (SiMe₃), 4.09 [d, *J*_{PC} = 54.7 Hz, CHP], 47.88 (NMe₂), 63.43 [d, *J*_{PC} = 17.3 Hz, CH₂N], 124.62, 130.44, 134.87, 140.27 (aryl). ³¹P{¹H} NMR (CD₂Cl₂, 20 °C): δ –41.1. ¹¹⁹Sn{¹H} NMR (CD₂Cl₂, 20 °C): δ 257 [d, *J*_{SnP} = 1070 Hz].

[[{(Me₃Si)₂CH}(C₆H₄-2-CH₂NMe₂)P]₂Sn (**8**). To a stirred solution of SnCl₂ (0.29 g, 1.57 mmol) in cold (–78 °C) THF (20 mL) was added a solution of [(Me₃Si)₂CH](C₆H₄-2-CH₂NMe₂)P]Li (1.04 g, 3.14 mmol) in THF (20 mL), excluding light as much as possible. The reaction mixture was allowed to attain room tem-

(25) Clegg, W.; Doherty, S.; Izod, K.; Kagerer, H.; O'Shaughnessy, P.; Sheffield, J. M. *J. Chem. Soc., Dalton Trans.* **1999**, 1825.

Table 1. Crystallographic Data for **5** and **8**

	5	8
formula	C ₁₆ H ₃₁ ClGeNPSi ₂	C ₃₂ H ₆₂ N ₂ P ₂ Si ₄ Sn
fw	432.6	767.8
cryst size, mm	0.40 × 0.22 × 0.20	0.38 × 0.36 × 0.20
cryst syst	monoclinic	triclinic
space group	<i>P</i> 2 ₁ / <i>c</i>	<i>P</i> $\bar{1}$
<i>a</i> , Å	19.1002(6)	12.7543(6)
<i>b</i> , Å	10.1387(3)	12.8444(16)
<i>c</i> , Å	11.5197(4)	25.4612(12)
α , deg		90.789(2)
β , deg	106.099(4)	90.187(2)
γ , deg		101.872(2)
<i>V</i> , Å ³	2143.32(12)	4081.4(3)
<i>Z</i>	4	4
ρ_{calcd} , g cm ⁻³	1.341	1.250
μ , mm ⁻¹	1.738	0.844
no. reflns measd	3740	34 437
no. unique reflns, <i>R</i> _{int}		18 159, 0.034
no. reflns with <i>F</i> ² > 2 σ (<i>F</i> ²)	3270	14 131
transm coeff range	0.543–0.723	0.740–0.850
<i>R</i> , <i>R</i> _w ^a (<i>F</i> ² > 2 σ)	0.047, 0.154	0.045, 0.104
<i>R</i> , <i>R</i> _w ^a (all data)	0.053, 0.156	0.064, 0.111
<i>S</i> ^a	1.149	1.049
refined params	209	740
max., min. diff map, e Å ⁻³	1.42, -0.54	1.88, -1.00

^a Conventional $R = \sum \|F_o\| - |F_c| / \sum \|F_o\|$; $R_w = [\sum w(F_o^2 - F_c^2)^2 / \sum w(F_o^2)^2]^{1/2}$; $S = [\sum w(F_o^2 - F_c^2)^2 / (\text{no. data} - \text{no. params})]^{1/2}$ for all data.

perature and was stirred for 16 h. Solvent was removed *in vacuo*, and the sticky brown solid was extracted into light petroleum (20 mL) and filtered. Solvent was removed *in vacuo* from the filtrate, and the sticky solid was recrystallized from cold (-30 °C) *n*-hexane as orange blocks of **8**. Yield: 0.94 g, 78%. Anal. Calcd for C₃₂H₆₂N₂P₂Si₄Sn: C, 49.40; H, 7.97; N, 3.72. Found: C, 49.29; H, 8.12; N, 3.66. ¹H NMR (*d*₈-toluene, 24 °C): δ 0.00 (18H, s, SiMe₃), 0.17 (18H, s, SiMe₃), 0.68 [2H, d, *J*_{PH} = 6.4 Hz, CHP], 2.13 (s, 12H, NMe₂), ~3.50 (br s, 2H CH₂N), 3.94 (s, 2H, CH₂N), 6.72–7.52 (m, 8H, aryl). ¹³C{¹H} NMR (*d*₈-toluene, 23 °C): δ 4.48 (SiMe₃), 7.67 (CHP), 48.79 (NMe₂), 64.98 [d, *J*_{PC} = 25.1 Hz, CH₂N], 125.34, 127.29, 130.58, 133.33, 139.40, 146.60 (aryl). ³¹P{¹H} NMR (*d*₈-toluene, 21 °C): δ -55.3 (s, br). ¹¹⁹Sn{¹H} NMR (*d*₈-toluene, 23 °C): δ 558 [t, *J*_{SnP} = 1045 Hz].

Crystal Structure Determinations of **5 and **8**.** Measurements were made at 150 K on Bruker SMART and Oxford Diffraction Gemini A Ultra diffractometers using graphite-monochromated Mo K α radiation ($\lambda = 0.71073$ Å). Cell parameters were refined from the observed positions of all strong reflections. Intensities were corrected semiempirically for absorption, based on symmetry-equivalent and repeated reflections. The structures were solved by direct methods and refined on *F*² values for all unique data. Table 1 gives further details. All non-hydrogen atoms were refined anisotropically, and H atoms were constrained with a riding model; *U*(H) was set at 1.2 (1.5 for methyl groups) times *U*_{eq} for the parent atom. The crystal of **5** was nonmerohedrally twinned (9.5(2)% minor component), preventing merging of equivalent reflections

before refinement because of reflection overlap. Programs were Bruker AXS SMART, SAINT, SHELXTL, Oxford Diffraction CrysAlisPro, and local programs.²⁶

DFT Calculations. Geometry optimizations and single-point energy calculations were performed on the gas phase molecules with the Gaussian03 suite of programs (revision C.02)²⁷ on a 224-core Silicon Graphics Altix 4700, with 1.6 GHz Montecito Itanium2 processors, via the EPSRC National Service for Computational Chemistry Software (<http://www.nscs.ac.uk>).

Ground state optimizations of the model compounds **7a** and **8a** were carried out using the B3LYP hybrid functional²¹ with an Lanl2dz effective core potential basis set²² for Sn and a 6-31G(d,p) all-electron basis set on all other atoms²³ [B3LYP/6-31G(d,p),Lanl2dz; default parameters were used throughout]. Transition states were initially located using the QST3 method at the HF/3-21G* level of theory prior to a full transition state geometry optimization at the B3LYP/6-31G(d,p),Lanl2dz level of theory. For several test cases final energies for **7a** and **8a** were further calculated at the MP2/6-31G(d,p),Lanl2dz level of theory;²⁸ energy differences obtained from these calculations differed only marginally from those calculated at the B3LYP/6-31G(d,p),Lanl2dz level of theory, and so only the latter energies were used. Minima were confirmed by the absence of imaginary vibrational frequencies and transition states by the presence of a single imaginary vibrational frequency; the accuracy of transition states was judged by consideration of the principal displacement vectors of the imaginary vibrational mode in each case. For direct comparison, final energies for **5a** were calculated at the B3LYP/6-31G(d,p) level of theory using previously reported optimized geometries.¹⁶

Acknowledgment. The authors are grateful to the Royal Society and the EPSRC for support. Dr. J. L. Bookham (Northumbria University) is thanked for access to the JEOL Eclipse270 NMR spectrometer.

Supporting Information Available: For **5** and **8** details of structure determination, atomic coordinates, bond lengths and angles, and displacement parameters in CIF format. For **7a** and **8a** details of DFT calculations, final atomic coordinates, and energies. Full details of ref 27. This material is available free of charge via the Internet at <http://pubs.acs.org>. Observed and calculated structure factor details are available from the authors upon request.

OM8011757

(26) (a) SMART and SAINT software for CCD diffractometers; Bruker AXS Inc.: Madison, WI, 1997. (b) CrysAlisPro; Oxford Diffraction Ltd.: Oxford, UK. (c) Sheldrick, G. *Acta Crystallogr., Sect. A* **2008**, *64*, 112.

(27) Frisch, M. J.; et al. *Gaussian 03, Revision C.02*; Gaussian, Inc.: Wallingford, CT, 2004.

(28) (a) Head-Gordon, M.; Pople, J. A.; Frisch, M. J. *Chem. Phys. Lett.* **1988**, *153*, 503. (b) Frisch, M. J.; Head-Gordon, M.; Pople, J. A. *Chem. Phys. Lett.* **1990**, *166*, 275. (c) Frisch, M. J.; Head-Gordon, M.; Pople, J. A. *Chem. Phys. Lett.* **1990**, *166*, 281. (d) Head-Gordon, M.; Head-Gordon, J. *Chem. Phys. Lett.* **1994**, *220*, 122. (e) Saebo, S.; Almlof, J. *Chem. Phys. Lett.* **1989**, *154*, 83.